Inorganic Chemistry
Article

Inorg. Chem. **2010**, *49*, 8017–8024 **8017**
DOI: 10.1021/ic101023b

The Magnetism of $(5MAP)_2CuBr_4$ [5MAP = 5-Methyl-2-aminopyridinium]: A Quasi-2D or a 3D Magnetic System?

Joaquim Jornet-Somoza,[†] Mercè Deumal,*[,†] Christopher P. Landee,[‡] Mark M. Turnbull,[‡] and Juan J. Novoa*[,†]

[†]*Departament de Química Física and IQTCUB, Facultat de Química, Universitat de Barcelona, Martí i Franquès 1, 08028-Barcelona, Spain, and* [‡]*Carlson School of Chemistry and Department of Physics, Clark University, Worcester, Massachusetts 01610*

Received May 20, 2010

In order to determine if its magnetic topology is actually two- or three-dimensional (2D or 3D), the mechanism of the magnetic interaction in $(5MAP)_2CuBr_4$, a previously thought quasi-2D antiferromagnet, is re-examined using the first-principles bottom-up methodology. Once the magnitude and sign of all unique magnetic interactions present in the room-temperature $(5MAP)_2CuBr_4$ crystal are evaluated, it is found that, even at room temperature, the magnetic topology of the crystal corresponds to a 3D antiferromagnet. Such 3D nature cannot be determined by examination of the magnetic susceptibility curve, $\chi(T)$, because it is found that the $\chi(T)$ curve computed using this 3D magnetic topology is very similar to that obtained using a 2D model where all interplane interactions have been deleted. However, its 3D magnetic dimensionality can be confirmed by examination of the shape of the magnetization curve, M(H); the computed curve is similar to the experimental one for the 3D case.

Introduction

Two-dimensional (2D) antiferromagnets are remarkable for their sensitivity to exchange anisotropy, remaining disordered at all temperatures in the case of isotropic (Heisenberg) exchange, but readily ordering at low temperatures for easy-plane or easy-axis anisotropies.[1] Therefore, within the framework of phase transitions, there has recently been a strong interest in understanding the magnetic properties of 2D $S = 1/2$ Heisenberg antiferromagnets (AFM). This has become especially important for the examination of a number of theoretical predictions, particularly those involving field-dependent properties.[2] However, this requires the preparation of 2D AFM systems presenting reasonably small intralayer exchange interactions, as most field-dependent studies are impossible on the La_2CuO_4 based family of superconductors where the strong intraplanar AFM interactions ($> |550|$ cm^{-1}) make it impossible to study the magnetism of the materials in an appreciable fraction of their saturation field.[3]

Many 2D AFM systems showing small (inter/intra)-layer exchange ratios have been prepared and characterized, both through structural isolation of layers within a crystal lattice[4] and via the use of thin films.[5] Even though these materials are predominantly 2D layered systems, they present weak interplane interactions, and a 2D-to-3D magnetic crossover is expected to occur at sufficiently low temperatures. Alternatively, 3D long-range order could arise within a layer due to a high anisotropy.[6] Despite such drawbacks, 2D systems showing weak intraplane exchange interactions may still serve as good approximations to 2D systems over a wide temperature range, provided that the ratio between the (inter/intra)-layer magnetic interactions is sufficiently small.[7]

*To whom correspondence should be addressed. E-mail: juan.novoa@ub.edu.

(1) De Jongh, L. J.; Miedema, A. R. *Adv. Phys.* **2001**, *50*, 947–1170.

(2) (a) Radu, T.; Tokiwa, Y.; Coldea, R.; Gegenwart, P.; Tylczynski, Z.; Steglich, F. *Sci. Technol. Adv. Mater.* **2007**, *8*, 406–409. (b) Chernyshev, A. L.; Zhitomirsky, M. E. *Phys. Rev. B: Cond. Matter Mater. Phys.* **2009**, *79*, 174402/1–5. (c) Syromyatnikov, A. V. *Phys. Rev. B: Cond. Matter Mater. Phys.* **2009**, *79*, 054413/1–6. (d) Cuccoli, A.; Gori, G.; Vaia, R.; Verrucchi, P. *J. Appl. Phys.* **2006**, *99*, 08H503/1–3.

(3) (a) Kastner, M. A.; Birgeneau, R. J.; Shirane, G.; Endoh, Y. *Rev. Mod. Phys.* **1998**, *70*, 897–928. (b) Birgeneau, R. J. *Am. J. Phys.* **1990**, *58*, 28–40.

(4) (a) Arimoto, Y.; Ohkoshi, S. I.; Zhong, Z. J.; Seino, H.; Mizobe, Y.; Hashimoto, K. *Chem. Lett.* **2002**, 832–833. (b) Albrecht, A. S.; Landee, C. P.; Slanic, Z.; Turnbull, M. M. *Mol. Cryst. Liq. Cryst.* **1997**, *305*, 333–340. (c) Turnbull, M. M.; Albrecht, A. S.; Jameson, G. B.; Landee, C. P. *Mol. Cryst. Liq. Cryst.* **1999**, *335*, 245–252.

(5) (a) Park, J.-H.; Culp, J. T.; Hall, D. W.; Talham, D. R.; Meisel, M. W. *Physica B* **2003**, *329−333*, 1152–1153. (b) Ohnuki, H.; Ishizaki, Y.; Suzuki, M.; Desbat, B.; Delhaes, P.; Giffard, M.; Imakubo, T.; Mabon, G.; Izumi, M. *Mater. Sci. Eng., C* **2002**, *C22*, 227–232.

(6) Bordallo, H. N.; Chapon, L.; Manson, J. L.; Hernandez-Velasco, J.; Ravot, D.; Reiff, W. M.; Argyriou, D. N. *Phys. Rev. B* **2004**, *69*, 224405/1–9.

(7) Coldea, R.; Tennant, D. A.; Tylczynski, Z. *Phys. Rev. B* **2003**, *68*, 134424/1–16.

(8) (a) Stefanyi, P.; Feger, A.; Orendaceva, A.; Chernyi, A. S. *Fiz. Nizkikh Temp. (Kiev)* **1990**, *16*, 224–234. (b) Brunner, O.; Karkut, M. G.; Antognazza, L.; Mieville, L.; Van der Linden, P.; Perenboom, J. A. A. J.; Triscone, J. M.; Fischer, O. *Physica C* **1991**, *185−189*, 2079–2080. (c) Pradhan, A. K.; Hazell, S. J.; Hodby, J. W.; Chen, C.; Hu, Y.; Wanklyn, B. M. *Physica C* **1993**, *218*, 208–12. (d) Radu, T.; Tokiwa, Y.; Coldea, R.; Gegenwart, P.; Tylczynski, Z.; Steglich, F. *Sci. Technol. Adv. Mater.* **2007**, *8*, 406–409. (e) von Ortenberg, M. *AIP Conf. Proc.* **2009**, *1147*, 14–21. (f) Rueff, J.-M.; Paulsen, C.; Souletie, J.; Drillon, M.; Rabu, P. *Solid State Sci.* **2005**, *7*, 431–436.

Published on Web 08/09/2010

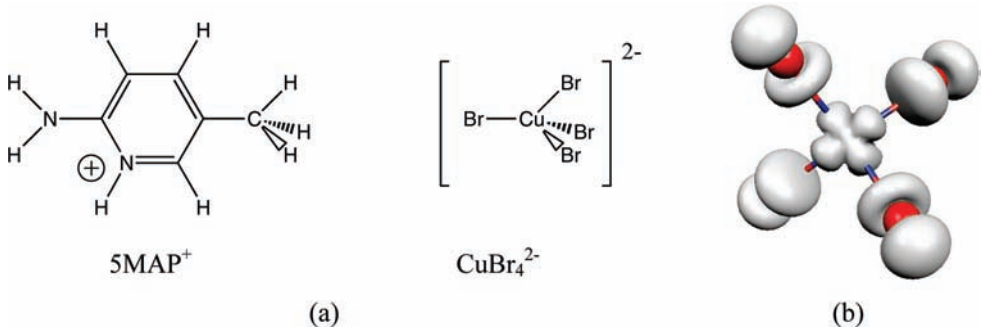

Figure 1. (a) Molecular geometry of $5MAP^+$ and $CuBr_4^{2-}$ ions. (b) Spin density of the $CuBr_4^{2-}$ ion (doublet ground state, plotted for the 0.002 au. isodensity surface; it is positive everywhere).

Over the past two decades, the properties of potential quasi-2D dimensional materials have been investigated in a variety of metal complexes, both experimentally[8] and theoretically.[9] The degree of interplanar isolation in these complexes has been measured by looking at the $T_N/2|J_{intra}|$ ratio, where T_N is the 3D-ordering temperature and J_{intra} is the magnetic exchange within the layers. It was found that even the best isolated 2D systems reported to date have figures of merit of $T_N/2|J_{intra}| \geq 0.17$.[10,11] Quantum Monte Carlo simulations have shown the effect of layer isolation on the properties of such magnetic systems as a function of the J_{inter}/J_{intra} ratio (J_{inter} and J_{intra} being the inter- and intralayer exchange interactions, respectively, with $J_{inter} < J_{intra}$).[12] At large values of J_{inter}/J_{intra}, a peak is observed in the specific heat, characteristic of the 3D-ordering transition. However, as the J_{inter}/J_{intra} ratio decreases, two distinct maxima are observed, one attributed to the establishment of short-range 2D order, and a second to 3D-ordering. The magnitude of the heat capacity anomaly becomes vanishingly small for values of J_{inter}/J_{intra} less than 0.2 making it difficult to identify the transition from 2D to 3D ordering in these systems.

The $(5MAP)_2CuBr_4$ compound (5MAP = 2-amino-5-methyl pyridinium, Figure 1a) is one of the recently reported compounds believed to present quasi-2D AFM properties and weak intraplanar exchange interactions.[13] $(5MAP)_2CuBr_4$ belongs to a family of Cu(II) salts with the general chemical formula A_2CuX_4, where A = 5MAP, 5CAP, or 5BAP (5CAP = 2-amino-5-chloropyridinium; 5BAP = 2-amino-5-bromopyridinium) and X = Br or Cl. By fitting the magnetic susceptibility curves to a pure 2D model (a 2D-QHAF quantum Heisenberg antiferromagnet), intraplane magnetic interactions of −3.0, −2.4, and −2.3 cm^{-1} were obtained for $(5CAP)_2CuBr_4$, $(5BAP)_2CuBr_4$, and $(5MAP)_2CuBr_4$, respectively.[13b,c,14] The saturation fields for these compounds were estimated to be 24.1, 19.6, and 18.8 T, respectively, thus making it possible to attain saturation in studies of their magnetization curves, M(H).

The magnetic susceptibility curves, $\chi(T)$, of $(5MAP)_2CuBr_4$ and $(5CAP)_2CuBr_4$ are well fitted using 2D models from room temperature to a temperature slightly below the maximum in $\chi(T)$ (∼5−8 K), whereupon their behavior deviates significantly.[13b,c] The deviation was thought to be due to the onset of interactions between the planes, that is, to a 2D−3D magnetic phase transition.[13c] The presence of long-range 3D order was observed for $(5CAP)_2CuBr_4$ via specific heat measurements.[14] The absence of a suitable model capable of describing such 2D-3D crossover left unanswered the question of just how strong the interlayer interactions were, although $T_N/2|J_{intra}|$ ratios of ∼0.6 for five A_2CuX_4 isomorphous complexes (when A = 5CAP or 5MAP, X = Br or Cl; when A = 5BAP, X = Br)[13] indicated that the interactions between layers must be significant in spite of the apparent correlation to the 2D-model above T_N. All these deficiencies prompted us to re-evaluate the mechanism of the magnetic interaction in $(5MAP)_2CuBr_4$ using a first-principles bottom-up procedure.[15] The first-principles bottom-up procedure calculates the value of all unique magnetic exchange pathways, $J(di)$, between the radicals in any molecule-based magnetic crystal from the only knowledge of the crystal structure, that is, without making any biased assumption on the strength or nature of the radical−radical magnetic interactions. Then, using these calculated magnetic interactions, the macroscopic magnetic properties (such as the magnetic susceptibility, magnetization, and heat capacity) are computed and their value and variation connected with the $J(di)$ pair interactions. The reliability of the first-principles bottom-up procedure has been demonstrated in both organic[16] and metal-based systems.[17] The computed

(9) (a) Mira, J.; Rivas, J. *Rev. - R. Acad. Galega Cienc.* **1999**, *18*, 35–58. (b) Olson, C. J.; Zimanyi, G. T.; Kolton, A. B.; Gronbech-Jensen, N. *Phys. Rev. Lett.* **2000**, *85*, 5416–5419. (c) Fridman, Yu. A.; Kosmachev, O. A.; Klevets, F. N. *Low Temp. Phys.* **2006**, *32*, 214–223. (d) Leon, H.; Estevez-Rams, E. *J. Phys. D: Appl. Phys.* **2009**, *42*, 185012/1–10.

(10) Greven, M.; Birgeneau, R.; Endoh, Y.; Kastner, M.; Matsuda, M.; Shirane, G. *Z. Phys. B: Condens. Matter* **1995**, *96*, 465.

(11) Navarro, R. *Magnetic Properties of Layered Transition Metal Compounds*; Jongh, L. D., Ed.; Kluwer Academic Press: Dordecht; p 105.

(12) Sengupta, P.; Sandvik, A. W.; Singh, R. P. *Phys. Rev. B* **2003**, *68*, 094423.

(13) (a) Place, H.; Willett, R. D. *Acta Crystallogr., Sect. C* **1987**, *C43*, 1050–3. (b) Woodward, F. M.; Landee, C. P.; Giantsidis, J.; Turnbull, M. M.; Richardson, C. *Inorg. Chim. Acta* **2001**, *324*, 324–330. (c) Woodward, F. M.; Albrecht, A. S.; Wynn, C. M.; Landee, C. P.; Turnbull, M. M. *Phys. Rev. B* **2002**, *65*(144412), 1–13.

(14) Matsumoto, T; Miyazake, Y.; Albrecht, A. S.; Landee, C. P.; Turnbull, M. M.; Sorai, M. *J. Phys. Chem. B* **2000**, *104*, 9993–10000.

(15) Deumal, M.; Bearpark, M. J.; Novoa, J. J.; Robb, M. A. *J. Phys. Chem. A* **2002**, *106*, 1299–1315.

(16) (a) Deumal, M.; Robb, M. A.; Novoa, J. J. *Polyhedron* **2005**, *24*, 2368–2376. (b) Deumal, M.; Bearpark, M. J.; Robb, M. A.; Pontillon, Y.; Novoa, J. J. *Chem.—Eur. J.* **2004**, *10*, 6422–6432. (c) Deumal, M.; Robb, M. A.; Novoa, J. J. *Polyhedron* **2003**, *22*, 1935–1944.

(17) (a) Deumal, M.; Giorgi, G.; Robb, M. A.; Turnbull, M. M.; Landee, C. P.; Novoa, J. J. *Eur. J. Inorg. Chem.* **2005**, 4697–4706. (b) Deumal, M.; Ribas-Ariño, J.; Robb, M. A.; Ribas, J.; Novoa, J. J. *Molecules* **2004**, *9*, 757–770. (c) Deumal, M.; Landee, C. P.; Novoa, J. J.; Robb, M. A.; Turnbull, M. M. *Polyhedron* **2003**, *22*, 2235–2239. (d) Li, L.; Turnbull, M. M.; Landee, C. P.; Jornet, J.; Deumal, M.; Novoa, J. J.; Wikaira, J. L. *Inorg. Chem.* **2007**, *46*, 11254–65. (e) Butcher, R. T.; Turnbull, M. M.; Landee, C. P.; Wells, B. M.; Novoa, J. J.; Ribas-Ariño, J.; Sandvik, A. W.; Awwadi, F. F. *Chem. Commun.* **2009**, 1359–61. (f) Shapiro, A.; Landee, C. P.; Turnbull, M. M.; Jornet, J.; Deumal, M.; Novoa, J. J.; Robb, M. A.; Lewis, W. *J. Am. Chem. Soc.* **2007**, *129*, 952–959. (g) Turnbull, M. M.; Landee, C. P.; Wells, B. M. *Coord. Chem. Rev.* **2005**, *249*, 2567–2576.

macroscopic property curves can also be compared with other curves obtained using hypothetical topologies, obtained by excluding some specific magnetic interactions from the calculation. This allows verification of the significance of these interactions (for instance, one can exclude all interlayer interactions in order to compare the 3D magnetic properties with those from a hypothetical 2D topology).

Computational Details

In order to perform a complete theoretical study of the magnetic properties of any molecule-based crystal, a working strategy, called the first-principles bottom-up procedure,[15] has been developed in our group. This procedure consists of the successive application of the following four steps:

Step 1. Analysis of the crystal packing in order to select all unique first- and second-neighbor radical-pairs, *di* (i.e., those not related by symmetry operations). The search for these radical-pairs is done by examining all pairs separated by less than a set cutoff distance, since it is known that the magnitude of the magnetic interaction decreases exponentially as the distance increases.

Step 2. Computation of the microscopic magnetic interactions, $J(di)$, for all unique radical-pairs selected in the previous step. The $(5MAP)_2CuBr_4$ crystal consists of $CuBr_4^{2-}$ doublet radicals composed of four diamagnetic Br^- ligands coordinated to one Cu(II), having one unpaired electron. The diamagnetic $(5MAP)^+$ cations play a structural and stabilizing role. Any radical−radical pair can either have a singlet or triplet electronic state, and the value of $J(di)$ for each pair is then obtained from the energy difference between the open-shell singlet (E_{BS}^{S}) and triplet (E^{T}) states. Both energies are computed using the B3LYP functional,[18] the Ahlrichs-pVDZ[19] basis set for Cu, and a 6-31+G(d)[20] basis set for the remaining atoms (as implemented in the Gaussian-03[21] code). For a proper description of the open-shell singlet, the broken symmetry approximation was used.[22] Within this approximation and using the $\hat{H} = -\sum_{i,j} 2J_{ij}\hat{S}_i\hat{S}_j$ expression of the Heisenberg Hamiltonian, the value of $J(di)$ is obtained as $2J(di) = 2(E_{BS}^{S} - E^{T})$[23] (this expression for $J(di)$ strictly derives from the original broken-symmetry equations[22] when the SOMO orbitals of the two radicals do not overlap). The use of this expression has been somewhat controversial for magnetic superexchange interactions, although it provides excellent results when compared to the experimental values in most cases.[24]

Step 3. Generation of the magnetic topology, defined by the network of non-negligible radical−radical magnetic connections within the crystal (any radical will be magnetically connected to its neighbor if their $J(di)$ is larger than $|0.05|$ cm^{-1}, a threshold value given by the precision of the calculation).[15] Given a magnetic topology, the minimal magnetic model is defined as the smallest subset of radicals that includes all non-negligible $J(di)$ interactions in a ratio as close as possible to that found in the infinite crystal. The repetition of this magnetic model along the crystallographic (a,b,c) directions should regenerate the magnetic topology of the full crystal (a useful test to check the validity of the selected magnetic model spaces).

Step 4. The radical centers constituting the magnetic models define a spin space that is used to compute the matrix representation of the corresponding Heisenberg Hamiltonian.[23] The energy and eigenvalues for all possible spin states of this Heisenberg Hamiltonian matrix can be computed using partial or full diagonalization methods. The size of the corresponding basis set increases with the number of doublet radical centers N of the magnetic model as $N!/[(N/2)!(N/2)!]$. Current computer limitations allow us up to 16 doublet centers for a full diagonalization and 30 doublet centers for a partial diagonalization (Lanczos method with partial reorthogonalization is used).[25] From the set of eigenvalues, one can then compute the macroscopic magnetic properties (heat capacity C_p, magnetic susceptibility χ, and magnetization M) using their statistical mechanics expression. These computed values can be then be compared with those obtained experimentally, or those computed using hypothetical magnetic topologies where one or more of the $J(di)$ interactions have user-assigned values (e.g., J(interplane) = 0).

Results and Discussion

1. Analysis of the $(5MAP)_2CuBr_4$ Crystal. As already indicated, the crystal structure of the $(5MAP)_2CuBr_4$ salt[13a] is made out of doublet ground state $Cu(II)Br_4^{2-}$ radical-anions and closed-shell (diamagnetic) $5MAP^+$ cations. They pack forming very dark brown-red crystals, in the monoclinic $C2/c$ crystallographic space group (at room temperature, a = 13.715 Å, b = 8.7162 Å, c = 16.013 Å, β = 93.79°). The $(5MAP)_2CuBr_4$ crystal can be visualized as the result of the stacking of identical *ac*-planes along the *b*-axis. Adjacent *ac*-planes are shifted in order to minimize like-charge contacts (Figure 2a). In these *ac*-planes, the $Cu(II)Br_4^{2-}$ radical-anions form rows along the *c*-axis, which are separated from each other by rows of $5MAP^+$ dimers that are placed in an up−down arrangement (Figure 2b). This allows the formation of short-distance Br···Br contacts (at 4.545 Å within the *ab*-planes and also at 4.973 Å between adjacent planes, see Figure 2c,d). Each $Cu(II)Br_4^{2-}$ radical-anion makes four in-plane interactions within the *ab*-plane, and four interplane interactions (Figure 2e). The short-distance in-plane Br···Br contacts create a 2D regular square-shaped network of interactions over the crystal ($d_{Br\cdots Br}$ = 4.545 Å) with $5MAP^+$ cations inserted between any two $Cu(II)Br_4^{2-}$ anions (Figure 2c). Each *ab*-plane is connected to its upper and lower adjacent plane by two identical 4.973 Å Br···Br contacts. The network that these short-distance Br···Br interactions build within the $(5MAP)_2CuBr_4$ crystal shows a 3D topology.

(18) (a) Becke, A. D. *Phys. Rev. A* **1988**, *38*, 3098. (b) Lee, C.; Yang, W.; Parr, R. G. *Phys. Rev. B* **1988**, *37*, 785. (c) Becke, A. D. *J. Chem. Phys.* **1993**, *98*, 5648.
(19) Schafer, A.; Horn, H.; Ahlrichs, R. *J. Chem. Phys.* **1992**, *97*, 2751.
(20) (a) Hariharan, P. C.; Pople, J. A. *Theor. Chim. Acta* **1973**, *28*, 213. (b) Francl, M. M.; Pietro, W. J.; Hehre, W. J.; Binkley, J. S.; Gordon, M. S.; DeFrees, D. J.; Pople, J. A. *J. Chem. Phys.* **1982**, *77*, 3654.
(21) Frisch, M. J. et al. *Gaussian-03, Revision-C.02*; Gaussian, Inc.: Wallingford, CT, 2004.
(22) (a) Noodlemann, L. *J. Chem. Phys.* **1981**, *74*, 5737. (b) Noodlemann, L. *Chem. Phys.* **1986**, *109*, 131.
(23) We have used the following general form of the Heisenberg Hamiltonian, as it is more convenient for our computer codes: $\hat{H} = -2\sum_{A>B} J_{AB}(\hat{S}_A\cdot\hat{S}_B + {}^1/_4\hat{I}_{AB})$ (1), where A and B indexes run over all non-negligible different radical-pairs in the minimal magnetic model space, $\hat{I}_{AB}$ is the identity operator, and $\hat{S}_A$ and $\hat{S}_B$ are the spin operators acting on radicals A and B of the A-B radical pair. It is worth pointing out that the energy spectrum computed using this Hamiltonian results in the same energy differences between different eigenvalues as those obtained using the more common expression: $\hat{H} = -2\sum_{A>B} J_{AB}\hat{S}_A\cdot\hat{S}_B$ (2).
(24) See for instance: (a) Ribas-Ariño, J.; Novoa, J. J.; Miller, J. S. *J. Mater. Chem.* **2006**, *16*, 2600. (b) Ruiz, E.; Alvarez, S.; Cano, J.; Polo, V. *J. Chem. Phys.* **2005**, *123*, 164110. (c) Adamo, C.; Barone, V.; Bencini, A.; Broer, R.; Filatov, M.; Harrison, N. M.; Illas, F.; Malrieu, J. P.; Moreira, I. P. R. *J. Chem. Phys.* **2006**, *124*, 107101. (d) Bencini, A.; Totti, F. *J. Chem. Theor. Comput.* **2009**, *5*, 144.
(25) Wilkinson, J. H. *The Algebraic Eigenvalue Problem*; Oxford University Press: Bath, Great Britain, 1988.

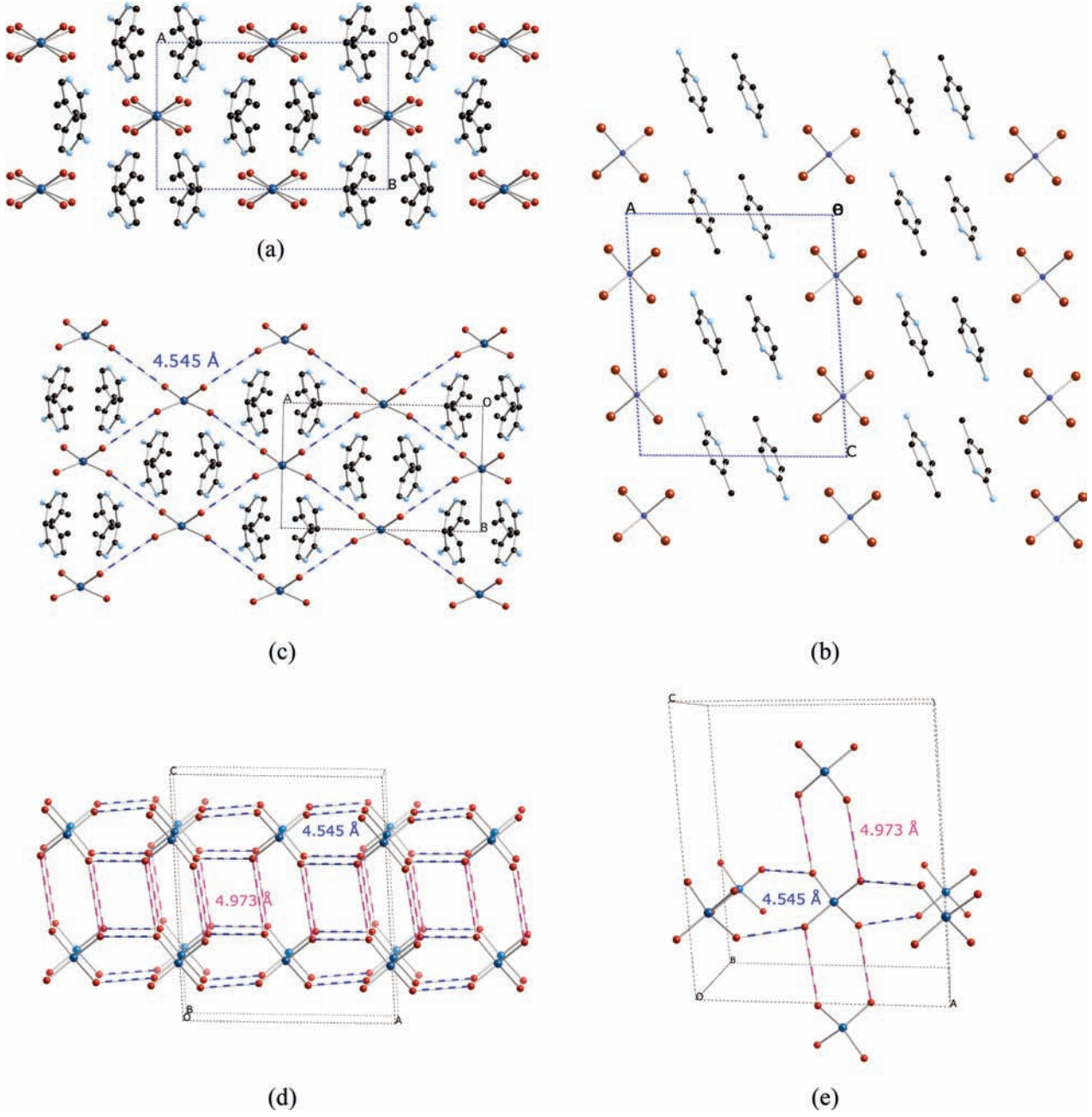

Figure 2. (a) View of the $(5MAP)_2CuBr_4$ crystal along the *c*-axis; (b) perpendicular view of one of the *ac*-planes. (c) View of the network formed by the 4.545 Å Br···Br contacts within the *ab*-plane. (d) Network built within the crystal by the 4.545 and 4.973 Å short-distance Br···Br contacts. (e) Br···Br short contacts made by any one $Cu(II)Br_4^{2-}$ anion within the crystal. All distances are in Å.

From the analysis of the packing of the room-temperature $(5MAP)_2CuBr_4$ crystal, it is possible to determine its unique radical-pairs. This was done by selecting those $Cu(II)Br_4^{2-}$ radical-anions whose Cu(II)···Cu(II) distance was shorter than 12.0 Å. Seven unique radical-pairs were found. The crystallographic arrangement of these unique radical-pairs and a detailed view of their geometry are depicted, respectively, in Figures 3 and S1 (Supporting Information).

The *d1* radical-pair connects two $Cu(II)Br_4^{2-}$ radicals of nearby *ab*-planes along the *c*-axis, and *d2* and *d3* connect radicals−anions within the *ab*-plane (*d3* along the *b*-axis). Radical-pairs *d4*, *d5*, *d6*, and *d7* connect nonvertical radical−anions of adjacent *ab*-planes, therefore, being relevant in establishing a 3D magnetic behavior by connecting the *ab*-planes. Table 1 shows the shortest Cu···Cu and Br···Br distances between the radicals of these seven pairs. Notice that while *d2* presents the shortest Br···Br distance, *d1* presents the shortest Cu···Cu distance. Looking only at the values of the shortest Cu···Cu distance, one would expect *d1*, *d2*, and *d3* to be the dominant magnetic interactions, but these three pairs cannot possibly define 2D magnetic layers as they would define a 3D magnetic topology. Therefore, the magnetic pathways in $(5MAP)_2CuBr_4$ will be driven by the relative orientation of $Cu(II)Br_4^{2-}$ radicals, which is the key factor determining the value of the magnetic interaction.[17g]

2. Calculation of the Magnetic Interaction for All Unique Radical-Pairs. The value of the magnetic exchange, *J*(*di*), for each unique radical-pair determined before was

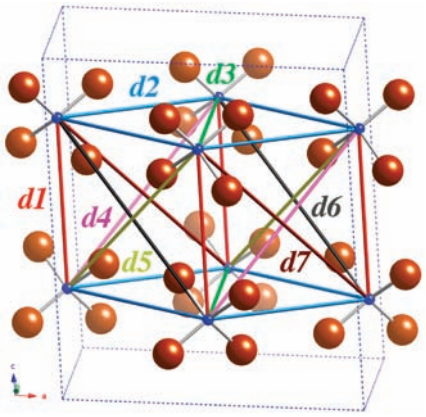

Figure 3. Crystallographic arrangement of the seven unique selected radical pairs in $(5MAP)_2CuBr_4$. Color lines are depicted to represent the possible magnetic connectivity (notice that these lines do not represent real bonds).

Table 1. Values of the Shortest Cu···Cu and Br···Br Distances for the *d1*−*d7* Radical-Pairs of the Room Temperature $(5MAP)_2CuBr_4$ Crystal[a]

pair, *di*	Cu···Cu/Å	Br···Br/Å	$J(di)/cm^{-1}$ $anion_2$ model	$J(di)/cm^{-1}$ $anion_2$−$cation_4$ model
d1	8.007	4.973	−2.85	−1.47
d2	8.125	4.545	−6.64	−3.35
d3	8.716	7.640	< |0.01|	
d4	11.073	8.328	< |0.01|	
d5	11.096	6.486	−0.15	−0.08
d6	11.710	6.978	−0.12	−0.07
d7	11.732	9.047	< |0.01|	

[a] The value of the $J(di)$ parameter for each pair is also given.

then computed. This evaluation can be done on the two isolated $CuBr_4^{2-}$ radicals that constitute the radical-pair, at their crystal geometry (i.e., using the $anion_2$ model in Table 1) or by also adding the nearest four $5MAP^+$ cations in each pair (the $anion_2$−$cation_4$ model in Table 1); the later model takes into account the main effects generated by the Madelung field.[26] Previous studies have shown that the presence of cations in the $anion_2$−$cation_4$ model localizes the anion-radical wave function more in space,[17] which results in a decrease in the overlap between the two radical wave functions. This leads to smaller $J(di)$ values for the non-negligible magnetic interactions (those where $J'(di) > |0.05|$ cm^{-1})[15] computed using the $anion_2$−$cation_4$ model. One expects the $anion_2$−$cation_4$ model to be closer to the experimental results, because this model reproduces better the experimental environment of the radicals within the crystal.

All non-negligible magnetic interactions in both models are antiferromagnetic, and their strength shows no correlation with the shortest Cu···Cu distance. Instead, it appears to show some correlation with the shortest Br···Br distance between the two radicals, with the $J(di)$ value also affected by the relative orientation of the radicals. This finding is consistent with the fact that the magnetic exchange in the $(5MAP)_2CuBr_4$ crystal occurs via through-space Cu−Br···Br−Cu pathways. This through-space interaction, caused by the overlap of the two $CuBr_4^{2-}$ radical wave functions, is made possible because the $CuBr_4^{2-}$ molecular orbitals are partially delocalized over the Br atoms. This also induces the delocalization of the unpaired electron density, located formally on the Cu(II) ion, over the Br atoms (see Figure 1b). It is also remarkable that non-negligible magnetic interactions exist in these through-space CuBr···BrCu interactions when the Br···Br distance is as great as 5.0 Å.

3. Determination of the Magnetic Topology. The magnetic topology of $(5MAP)_2CuBr_4$ is the network of magnetic interactions generated by the four non-negligible $J(d1)$, $J(d2)$, $J(d5)$, and $J(d6)$ interactions. The strongest magnetic interactions, $J(d1) = -1.47$ cm^{-1} and $J(d2) = -3.35$ cm^{-1}, generate a 3D network (see Figure 4a): $J(d2)$ forms regular square layers within the *ab*-plane, and $J(d1)$ connects any two directly aligned radicals of these layers along the *c*-axis. The two remaining magnetic interactions, $J(d5)$ and $J(d6)$, serve only to create weaker connections between adjacent *ab*-planes (see Figure 4a).

4. Computation of the Macroscopic Magnetic Properties. A proper magnetic model, whose expansion along the three crystallographic axes is capable of generating the magnetic topology of the full $(5MAP)_2CuBr_4$ crystal in an even way, is the 3D8s model (3D8s stands for its three-dimensional nature, and for the eight radical centers) (see Figure 4b). Calculations were also done with larger models, where the number of radical centers was enlarged from 8 to 16 (see Supporting Information Figure S2 for a variety of magnetic model spaces and S3 for the corresponding computed $\chi(T)$ data), in order to check the convergence of the computed $\chi(T)$ curves toward the experimental curve. All computed $\chi(T)$ curves do converge toward the 3D16s model data (see Figure 4c), which is taken as our minimal magnetic model. Therefore, from now on for discussion purposes we will refer to results computed with the 3D16s minimal model.

Using as a basis set the space of spin functions of the 16 doublet centers comprising the 3D16s model, the matrix representation of the Heisenberg Hamiltonian was built and diagonalized. The energies that result from that diagonalization were then used in the appropriate statistical mechanics expression[15] to compute the magnetic susceptibility curve, $\chi(T)$, of the $(5MAP)_2CuBr_4$ crystal (Figure 5). A comparison of the 3D16s computed $\chi(T)$ curve and the available experimental curve (either raw data, or experimental data fitted using a 2D QHAF model[13b] in Figure 5) indicates that the computed curve reproduces the main features of the experimental and fitted curves. The small deviation in the region of the maxima of $\chi(T)$ can be associated with the use of a room temperature crystal structure in the calculations, which is the only available crystal structure (temperature effects on the computed magnetic susceptibility curves have been extensively evaluated in other systems,[17d,f] concluding that thermal expansion induces nonisotropic changes in the $J(di)$ values; the agreement between experimental and computed curves is always improved if the temperature at which the crystal structure is determined is closer to the temperature at which the experimental curve shows its maximum[16,17]).

5. Magnetic Properties of a Hypothetical Purely 2D $(5MAP)_2CuBr_4$ Crystal. The similarity described above for $(5MAP)_2CuBr_4$ among the 2D-fitted $\chi(T)$ curve, the

(26) Kittel, C. *Introduction to Solid State Physics*, 7th ed.; John Wiley & Sons, Inc.: New York, 1996.

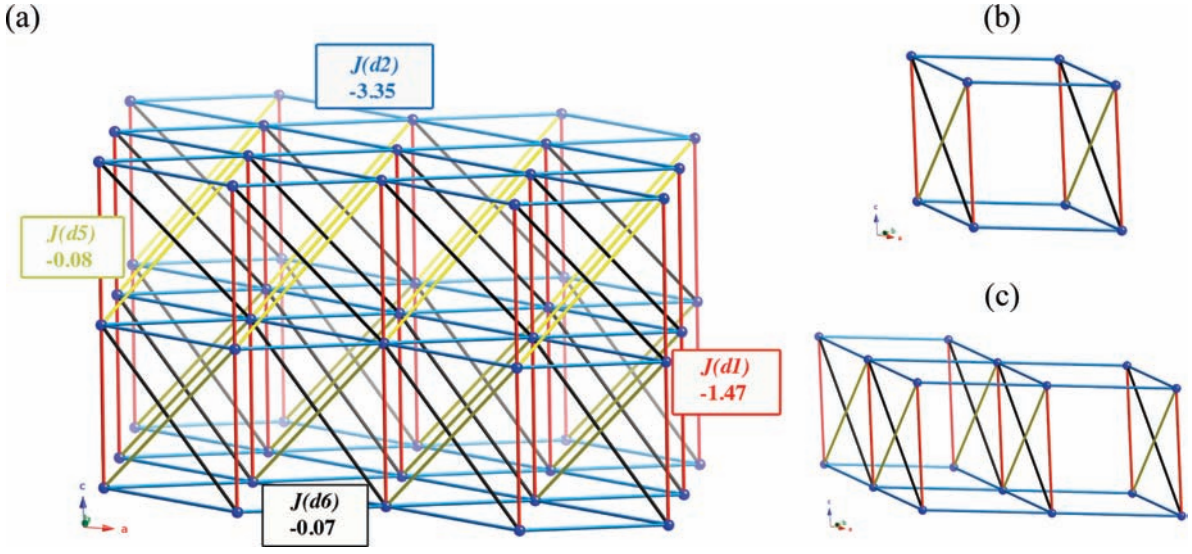

Figure 4. (a) Magnetic topology of the $(5MAP)_2CuBr_4$ crystal at room temperature (the values of the $J(di)$ interactions are given in cm^{-1}). (b) Representation of the 3D8s magnetic model. (c) Representation of the 3D16s magnetic model. In these drawings, each $CuBr_4^{2-}$ radical is represented by its centroid (no $5MAP^+$ cations are shown, for simplicity).

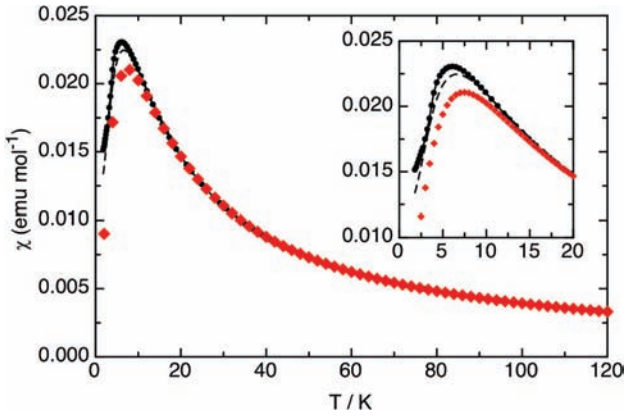

Figure 5. Comparison between experimental $\chi(T)$ curve and computed $\chi(T)$ curve using the three-dimensional 3D16s magnetic model (raw data: filled black circles; fitted values to a 2D QHAF model: dashed line; computed curve using the 3D16s model: red rhombus). The inset shows an expanded view of the maxima region.

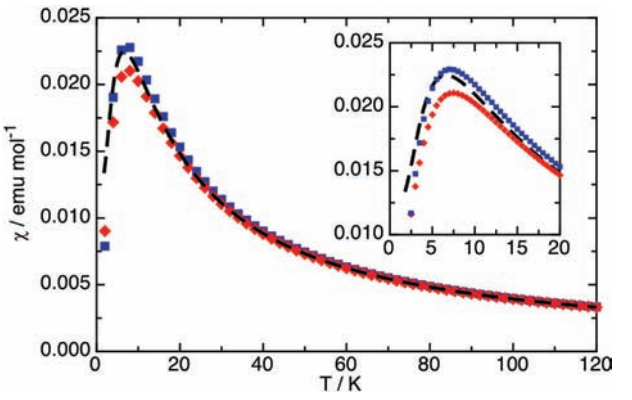

Figure 6. Comparison between experimentally fitted $\chi(T)$ curve and computed $\chi(T)$ curve using the three-dimensional 3D16s and two-dimensional 2D2x8s magnetic models (experimentally fitted values to a 2D QHAF model: dashed line; computed curve using the 3D16s model: red rhombus). The inset shows an expanded view of the maxima region.

raw data $\chi(T)$ curve (which, as was demonstrated above, corresponds to a 3D magnetic topology), and the $\chi(T)$ curve computed using the three-dimensional 3D16s model, prompted us to further investigate the magnetic properties of a hypothetical purely 2D magnetic topology obtained from the 3D16s model by setting the interplane $J(di)$ interactions equal to zero and recalculating the $\chi(T)$ curve. When the three non-negligible interplane interactions connecting adjacent *ab*-planes, $J(d1)$, $J(d5)$, and $J(d6)$, are deleted in the 3D16s minimal magnetic model, one obtains the 2D2x8s model, which is a two-dimensional model made out of two isolated planes, each constituted by eight doublet centers (see Figure 4c). The $\chi(T)$ curves computed using the 2D2x8s and 3D16s models have a similar shape (Figure 6), the main difference being the value of χ in the T_{max} region, which is larger using the 2D2x8s model. The $\chi(T)$ experimental raw data curve sits closely in between the 2D2x8s and 3D16s curves. This fact, added to the similarity between the raw-data and 2D-fitted curves, allows the conclusion that in $(5MAP)_2CuBr_4$ one cannot discriminate between 2D or 3D magnetic topologies solely by examining the shape of the magnetic susceptibility curve.

The origin of the similar shape of $\chi(T)$ using 3D16s and 2D2x8s models was further investigated around $\chi(T_{max})$. As shown in eq 1, the values of $\chi(T)$ are determined, besides some constants, by the $E_n - E_0$ differences and the spin S multiplicity of states n and 0.

$$\chi = \frac{Ng^2\mu_B^2}{3k_BT}\mu_0 \left[\frac{\sum_n S_n(S_n+1)(2S_n+1)\exp[-(E_n-E_0)/k_BT]}{\sum_n (2S_n+1)\exp[-(E_n-E_0)/k_BT]}\right] \quad (1)$$

As shown in Figure 7a, the full energy spectrum ΔE of the 3D16s and 2D2x8s magnetic models is similar. The analysis of the Boltzmann population at 7.5 K, which is the T_{max} of the χ curves, shows that only those states with $\Delta E \sim < 30\ cm^{-1}$ present a non-negligible population (see

Figure 7b). Therefore, in a qualitative analysis, the small differences in the ΔE values and in the population of these states suggest that these two models should present similar $\chi(T)$ curves around 7.5 K, as is the case. This explains why one cannot discriminate between 2D or 3D magnetic topologies solely by examining the shape of the magnetic susceptibility curve.

As already suggested in the experimental study,[13c] one can examine other magnetic properties, as heat capacity $C_p(T)$ or magnetization M(H) curve, in order to properly determine the magnetic dimensionality of $(5MAP)_2CuBr_4$. Figure 8 shows the $C_p(T)$ and M(H) curves computed using the 2D2x8s and 3D16s models. The two $C_p(T)$ curves (Figure 8a) are slightly different: the curve computed using the 3D16s model shows a small shoulder not observed in that computed with the 2D2x8s model (no comparison is possible with the experimental curve because it has not yet been measured for $(5MAP)_2CuBr_4$). However, such a result agrees with other theoretical works.[12] The M(H) curves computed using the 3D16s model (Figure 8b) is also different than that obtained with the 2D2x8s model: while the 2D2x8s curve presents shoulders in some fields (~10 and 14 T) not observed experimentally, the 3D16s data reproduces the linear increase found in the experimental curve in all regions except at very low magnetic fields, where the computed M becomes zero at values below ~2 T. An analysis of such behavior indicates that this is an unphysical trend, which is the consequence of the necessity for reasonably small finite magnetic model spaces in our calculations.

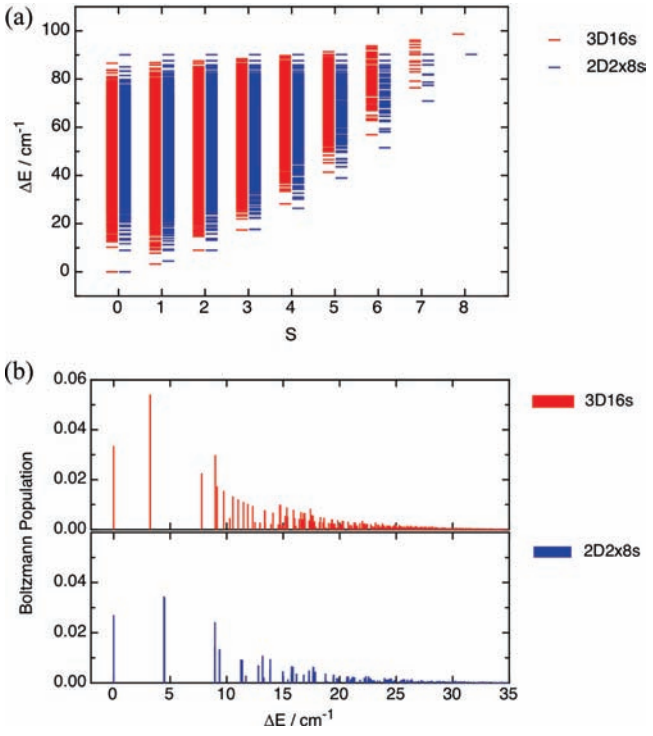

Figure 7. (a) Energy spectra ΔE as function of the S spin multiplicity for all states of the 3D16s and 2D2x8s magnetic models; (b) Boltzmann population at 7.5 K (maximum of $\chi(T)$ curves) of the lowest energy states of the same models.

Conclusions

A first-principles bottom-up study done on the room-temperature crystal structure of $(5MAP)_2CuBr_4$ shows that its magnetic topology is 3D even at room temperature. This 3D magnetic topology results from through-space Cu−Br···Br−Cu pathways that result from the overlap of $CuBr_4^{2-}$ orbitals. Four non-negligible antiferromagnetic $J(di)$ magnetic interactions are found, with values −1.47, −3.35, −0.08, and −0.07 cm^{-1}. The largest $J(di)$ interaction links the radicals within the *ab*-plane, forming a square magnetic lattice topology. Adjacent *ab*-planes are connected along the *c*-axis by the remaining three magnetic interactions. These are all through-space interactions, found to be significant even when the shortest Br···Br distances are about 5 Å.

The magnetic susceptibility curve, $\chi(T)$, computed using a three-dimensional model space, 3D16s, properly reproduces the shape of the experimental $\chi(T)$ curve, with a small deviation in the region of the curve maximum. This deviation can be ascribed to the use of a room-temperature crystal structure, in agreement with previous results on other molecule-based crystals. However, the $\chi(T)$ curve computed using a hypothetical pure 2D magnetic topology model obtained by deleting all inter *ab*-planes interactions also reproduces well the experimental $\chi(T)$ curve. Consequently, it can be safely

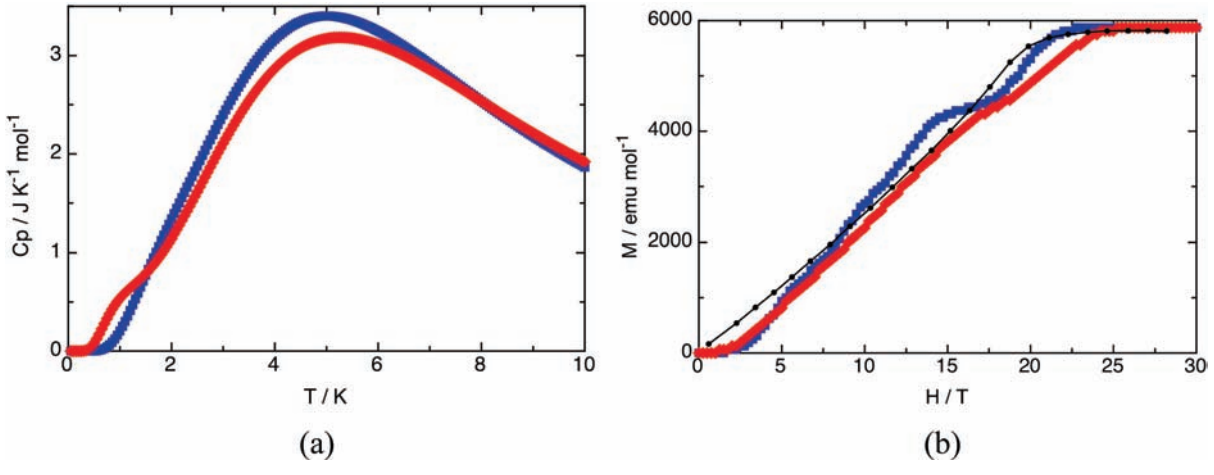

Figure 8. Comparison between the heat capacity (a) and magnetization (b) curves computed on the room-temperature $(5MAP)_2CuBr_4$ crystal using the three-dimensional 3D16s model (red rhombus) and a hypothetical two-dimensional 2D2x8s magnetic model (blue squares). The black dots in (b) are representative data points collected at 1.3 K (ref 13c).

concluded that one cannot assign the dimensionality of the magnetic topology in $(5MAP)_2CuBr_4$ by looking only at the shape of the $\chi(T)$ curves.

A comparison of the computed and experimental magnetization curves, M(H), indicates that the dimensionality can be assigned when examining the shape of these curves, as only the curves for 3D model spaces reproduce the main features of the experimental M(H) curve (except in the region of magnetic fields close to zero, due to the use of finite model spaces). No conclusions can be drawn on the heat capacity curve, $C_p(T)$, as there is no experimental data for this property on $(5MAP)_2CuBr_4$. However, computed $C_p(T)$ using the 3D16s model space shows a small shoulder at low temperatures ($T \sim 1$ K), which has been theoretically predicted to exist only on 3D models.

Overall, these results indicate that in order to make a proper assignment of the dimensionality of the magnetic topology in $(5MAP)_2CuBr_4$ (and, therefore, a correct interpretation of the mechanism of the magnetic interactions in this system) one cannot solely resort to magnetic susceptibility curves but needs further support. This support is 2-fold: experimental and theoretical. It can be obtained from other macroscopic magnetic observables, in this case, the M(H) curve, or from more sensitive experiments (such as muon spin rotation, μ-SR, studies). It can also be obtained by doing a first-principles bottom-up theoretical study of the crystal.

Acknowledgment. The team from Universitat de Barcelona would like to thank the support of the Spanish Spanish Science and Innovation Ministry (MAT2008-02032/MAT-FEDER Fonds cofinanced, and UNBA05-33-001; J.J.-S. also acknowledges his Ph.D. grant), the CIRIT (2009 SGR 1203), and CESCA and BSC for computer time. We would like to thank S. Kimber for support with the neutron diffraction experiment. The U.S. team is grateful for grants from the NSF (IMR-0314773) and the Kresge Foundation toward the purchase of the MPMS SQUID magnetometer.

Supporting Information Available: Complete ref 21. Figure S1: Geometry of the seven unique radical-pairs present in the $(5MAP)_2CuBr_4$ crystal (the Cu···Cu distance is indicated in each pair). Also the $anion_2-cation_4$ model for *d1*, *d2*, *d5*, and *d6* non-negligible radical pairs is given. The position of the four $5MAP^+$ counterions has been decided in terms of close contacts and symmetry. Figure S2. Three-dimensional magnetic models tested in our study: (a) 3D8s, (b) 3D12s_3x2x2, (c) 3D14s, (d) 3D16sZiZa, (e) 3D16s_4x2x2, (f) 3D12s_2x2x3. Figure S3. (a) Magnetic susceptibility data computed using three-dimensional magnetic models of Figure S2 (3D8s, 3D12s_3x2x2, 3D14s, 3D16sZiZa). (b) Magnetic susceptibility data computed using the same three-dimensional models and the hypothetical 2D models obtained from them by deleting J(*d1*), J(*d5*), and J(*d6*) inter *ab*-plane interactions. This material is available free of charge via the Internet at http://pubs.acs.org.